Journal of Materials Chemistry B

Accepted Manuscript

ROYAL SOCIETY OF CHEMISTRY

www.rsc.org/materialsB

Journal of Materials

Chemistry B

RSCPublishing

ARTICLE

Facile Preparation of Gadolinium(Ⅲ) Chelates Functionalized Carbon Quantum Dots-based Contrast Agent for Magnetic Resonance/ Fluorescence Multimodal Imaging

Cite this: DOI: 10.1039/x0xx00000x

Received 00th January 2012,
Accepted 00th January 2012

DOI: 10.1039/x0xx00000x

www.rsc.org/

Xianyan Ren,[a,b] Lihua Liu,[c] Yu Li,[a] Qin Dai,[c] Ming Zhang,[c] and Xinli Jing*[a]

Suffering from high inherent toxicity generated from heavy-metal in semiconductor quantum dots and complex preparation process, the medical application of conventional gadolinium(Ⅲ)/semiconductor quantum dots based magnetic resonance/fluorescence multimodal imaging (MRI/FI) contrast agent was limited. In this paper, a new kind of biocompatible carbon quantum dots functionalized by gadolinium(Ⅲ) chelates (named as Gd(Ⅲ)/CQDs) were obtained through one step pyrolysis of gadopentetate monomeglumine which provides simultaneously the carbon source and gadolinium(Ⅲ) source. The Gd(Ⅲ)/CQDs show good magnetic resonance response and photoluminescence properties, with longitudinal relaxation rate and quantum yield locating in 5.5-6.4 $mM \cdot L^{-1} \cdot S^{-1}$ [Gd(Ⅲ)%, 0.5mM] and 2.6-8.9%, respectively. The Gd(Ⅲ)/CQDs with diameters in the range of 2-3 nm can be well dispersed in deionized water, phosphate-buffered saline buffer solution or culture medium to form a stable dispersion, which with low cytotoxicity can penetrate into cells and show green fluorescence (excitation at 488 nm) presenting a great potential to be used as a MRI/FI contrast agent.

1. Introduction

Magnetic resonance/fluorescence multimodal imaging (MRI/FI) technology has an outstanding advantage of simultaneously offering both high-resolution histological information and high-sensitive functional imaging.[1-3] The development of MRI/FI contrast agents has been the hotspot in the fields of medicine and materials, in which the research on contrast agents constructed with gadolinium(Ⅲ) [Gd(Ⅲ)] chelates and semiconductor quantum dots (QDs) has attracted the greatest attention. On account of its characteristic of accelerating the longitudinal relaxation rate (r_1), Gd (Ⅲ) exhibits bright contrast, which with lowered cytotoxicity has been clinically used widely after coordination to polydentate chelator, e.g., DTPA and DTTA.[4, 5] Semiconductor QDs have distinguished emission profiles such as composition- and size-dependent absorption and emission, long fluorescence lifetime.[3, 6] In recent years, new nanoscale materials in addition to advanced nanotechnologies have provided ways of preparing novel MRI/FI contrast agents by conjugating semiconductor QDs with paramagnetic Gd(Ⅲ) chelates.[7-10]

The high cytotoxicity of semiconductor QDs limits the medical application of Gd(Ⅲ) chelates/semiconductor QDs based MRI/FI contrast agents and makes the process of constructing such contrast agents complicated. To date, several mechanisms have been postulated to illustrate the cytotoxicity of semiconductor QDs, including desorption of free Cd^{2+} (in the case of cadmium-based QDs), free radical formation, and the interaction of QDs with intracellular components.[11] Generally, the cytotoxicity of semiconductor QDs can be lowered by being coated with shells such as silica or functionalized silica. Yang *et al.* fabricated a Gd(Ⅲ) functionalized silica-coated CdS:Mn/ZnS MRI/FI contrast agent through two steps.[10] However, the silica encapsulation not only makes the synthesis more complex and difficult, but also increases the particle's size by a value of 4-7 nm.

Owning to their superb emission profiles and nontoxic nature, carbon quantum dots (CQDs) possibly could take the place of semiconductor QDs to become the next generation materials for building MRI/FI contrast agents. In 2009, Sun and his co-workers demonstrated that the CQDs injected in various ways into mice retained strong fluorescent, which might be used for optical imaging and related biomedical application.[12] Although CQDs have been used for sensitive detection, optical imaging and photothermal therapy,[12-14] only limited examples of CQDs based MRI/FI contrast agents are available. Bourlinos *et al.* prepared Gd(III)-doped CQDs as MRI/FI contrast agents through pyrolysis by employing tris(hydroxymethyl)-aminomethane as a carbon source and gadopentetic acid as a Gd(Ⅲ) source separately.[15] However, the precursors must undergo complex pretreatment procedures before pyrolysis, as well as neither the quantitative properties [including the

quantum yield (QY) and the r_1] nor the doping form of the resulting Gd(III)-doped CQDs were declared.

In this paper, a new kind of biocompatible Gd(Ⅲ) chelates functionalied CQDs [named as Gd(Ⅲ)/CQDs] are obtained by one-step pyrolysis of gadopentetate monomeglumine (GdPM) which serves as the precursor and is able to simultaneously provide both the carbon source and Gd(Ⅲ) source. GdPM is composed of gadopentetic acid (GdPA) and meglumine (Meg) units. During heating, those units exhibit obvious different thermal stability. By selecting appropriate pyrolysis temperatures through the analysis of the TGA process of GdPM, the Gd(Ⅲ)-N-O cyclic chelate structure in GdPA unit will not decompose conspicuously, meanwhile, the Meg unit is carbonized and generates nano-sized carbonaceous cores. Moreover, on the basis of experiments and analyses, we find that the Gd(Ⅲ)-N-O cyclic chelate structure as a functional surface will decorate the carbonaceous cores at a molecular level. Furthermore, compared with the precursor in Ref [15], the GdPM is a pharmaceutical intermediate of clinical magnevist MRI contrast agent, which provides potential biocompatibility for the Gd(Ⅲ)/CQDs. Finally, the dependence of structure and properties (i.e. QY, r_1) on pyrolysis temperature of Gd(Ⅲ)/CQDs were studied.

2. Experimental

2.1. Pyrolysis

As a precursor, GdPM was pyrolyzed through a process as follows: an alumina crucible with 1.5 g of GdPM was heated under a certain temperature for 2h in a tube furnace constantly purged with nitrogen. After naturally cooled to room temperature, a brown powder was obtained and named as Py-GdPM. The heating rate is 10 ^{o}C/min in the stage from room temperature to the preconcerted temperature.

GdPA, Meg and their equimolar mixture (Mx) were respectively pyrolyzed at sole 300 ^{o}C to obtain their pyrolytic products, named as Py-GdPA, Py-Meg and Py-Mx, correspondingly. Before the pyrolysis, the Mx was ground in a mortar to ensure that the GdPA and Meg were uniformly mixed.

All precursors (produced by Shandong Hongfuda Pharmchem Co., Ltd) were used without further purification.

2.2. The Separation of Py-GdPM and Preparation of CQDs (Gd(Ⅲ)/CQDs)

The Py-GdPM was dispersed into deionized water and vacuum filtered with a 0.22 μm microfiltration membrane using a Buchner funnel. The filter cake was discarded and yellow filtrate was collected. Then the obtained yellow filtrate was adjusted to pH 9 with NaOH and centrifuged at 8000 rpm. Finally, pure CQDs were obtained by concentrating the supernate and followed drying at 50 ^{o}C in vacuum oven. The yield of CQDs was presented as the mass ratio of the pure CQDs relative to the GdPM before pyrolysis (i.e., 1.5 g).

2.3. Characterization

In order to preliminarily determine the temperature for the pyrolysis of GdPM, thermogravimetric analysis (TGA) was performed at heating rate of 10 ^{o}C/min by TG209C thermogravimetric analyzer (NETZSCH). The chemical environment of Gd(Ⅲ) was confirmed by X-ray photoelectron spectroscopy (XPS, K-Alpha, Thermo Scientific Company). The structure of Gd(Ⅲ)/CQDs was analyzed by an infrared spectrometer (IR, Bruker TENSOR 27), an X-ray diffractometer (XRD, Bruker D8Advance) and an ultraviolet-visible spectrophotometer (UV-vis, Hitachi U2001). The Gd(Ⅲ) content was determined by an inductively coupled plasma optical emission spectrometer (ICP-ES, Varian 715). The particle size of Gd(Ⅲ)/CQDs was studied with JEOL JEM-2100 high resolution transmission electron microscopy (HRTEM, 200 kV).

2.4. Photoluminescence Properties

The excitation and emission spectra ($\lambda_{excitation}$=350 nm) of Gd(Ⅲ)/CQDs were collected with a FLsp920 fluorescence spectrophotometer (Edinburgh Instruments). The QY was determined by comparing the integrated PL emission spectral intensity ($\lambda_{excitation}$=365 nm) and the absorption value (at λ=365 nm) of Gd(Ⅲ)/CQDs using quinine sulfate (QY_R=0.55) in 0.1M H_2SO_4 (η=1.33)[16] as a reference. The QY was calculated according to Equation (1):[17]

$$QY = QY_R \frac{I}{I_R}\frac{A_R}{A}\frac{\eta^2}{\eta_R^2}. \quad (1)$$

Where A is the absorbance at the excitation wavelength, η is the refractive index of the solvent (for present case η/η_R=1), and I is the integrated emission intensity calculated from the area under the emission peak on the same wavelength scale.

2.5. Relaxometric Measurement

The T_1-weighted images and the longitudinal relaxation rate (r_1 /mM·L^{-1}·S^{-1}) of Gd(Ⅲ)/CQDs were measured, and compared with clinical magnevist MRI contrast agent with the same concentration of Gd(Ⅲ) (0.5 mM). Furthermore, a Gd(Ⅲ)/CQDs dispersion with Gd(Ⅲ) concentration of 1.0 mM was made and further diluted to different Gd(Ⅲ) concentrations (0.1, 0.2, 0.4, 0.8, 1.0 mM) to investigate the relationship between Gd(Ⅲ) concentration and MR response (i.e., brightness of T_1-weighted images, longitudinal relaxation times T_1). To calculate the r_1 of the Gd(Ⅲ)/CQDs, T_1 was measured first with a 3.0 T MRI scanner (GE Medical Systems). T_1-weighted images were obtained with a SE sequence (TR/TE= 300 ms/20 ms, Matrix 256×256 pixel, FOV 24 cm×24 cm, NEX 1, slice thickness of 5 mm, gap 1.5 mm). In order to acquire the T_1 values, inversion recovery sequence was used, applying three different TI (TI=100, TI=300, TI=600, TR/TE 4000 ms/9.2 ms). The r_1 was estimated based on Equation (2):[18]

$$(1/T_1)_{obsd}=(1/T_1)_{dia}+r_1\times[M]. \quad (2)$$

Where $(1/T_1)_{obsd}$ is the observed relaxation rate of water proton in the presence of paramagnetic species, $(1/T_1)_{dia}$ is the relaxation rate in the absence of the paramagnetic species and $[M]$ is the molar concentration of the paramagnetic species.

2.6. Cytotoxicity

The cytotoxicity of the Gd(Ⅲ)/CQDs was assessed on HeLa cells and was performed through the CCK-8 assay (Signalway Antibody, SAB).[19] HeLa cells were planted in the 96-well plates (0.5×10^4 cell per well) and then cultured with RPMI 1640 (Hyclone) in a humidified incubator with 5% CO_2 at 37 ^{o}C. After an incubation period of 24 h, different concentration (10, 20, 40, 80, 100, 200 μg·mL^{-1}) of the Gd(Ⅲ)/CQDs were added to each well of the 96-well plates. And cells cultured in the medium without Gd(Ⅲ)/CQDs were taken as the control. After incubation for another 24h, CCK-8 solution was added to each well and incubated for 4h at 37 ^{o}C, the optical density (OD) of each well was measured with a Microplate Reader at 450 nm. The *cell viability (%)=(OD_{sample} – OD_{blank}) / ($OD_{control}$*

$– OD_{blank}) \times 100\%$,[20] where the subscript *blank* is the wells without HeLa cells.

For phototoxicity study, the HeLa cells were prepared as described above and incubated with 50 μg·mL^{-1} Gd(Ⅲ)/CQDs. The cells were then exposed to blue light (470 nm-480 nm, 1W) for 5 min and 10 min, respectively, and further cultured for 30 h. The distance between bottom of the cuvette with sample and the lamp was 1 cm, and the irradiation intensity was 3.1 W/cm^2. Phototoxicity results were presented as percentage of the viability of HeLa cells that exposed to light relative to the cells not exposure to the light. In order to clarify whether Gd(Ⅲ)/CQDs would introduce more phototoxicity to cells, the phototoxicities toward HeLa cells incubated with and without Gd(Ⅲ)/CQDs were tested.

2.7. Fluorescence Imaging

HeLa cells were grown in RPMI with 10% heat-inactivated fetal bovine serum at 37 °C in 5% CO_2. Cells (0.3×10^5) were seeded on cover slips in a tissue culture dish in RPMI1640 culture medium (5 mL). When the culture dish was at least 80% confluent, Gd(Ⅲ)/CQDs (prepared at 300 °C, with weight extinction coefficient of 1.99 L·g^{-1}·cm^{-1} and 0.72 L·g^{-1}·cm^{-1} at 365 nm and 488 nm, respectively) in concentrations of 50 ug·mL^{-1} and 200 ug·mL^{-1} were separately added followed by incubation for 20 h. Cover slips were removed from a culture Petri dish with scalpels and washed three times with phosphate-buffered saline (PBS), followed by fixation with 2% paraformaldehyde (10 min). They were mounted on glass slides for observation in a fluorescence microscope (Olympus BX51, Tokyo) with excitation wavelength at 488nm. The weight extinction coefficients of Gd(Ⅲ)/CQDs were measured according to Lambert-Beer law and detailed method was shown in ESI, and the related data were shown in Fig.S1.

3. Results and Discussion

3.1. Pyrolysis Process

As a small aliphatic organic molecule, Meg can decompose even at low temperatures like citric acid, glucose and L-lysine which have been widely employed as precursors to prepare CQDs via partial pyrolysis.[14, 16, 21] TGA curve 1 in Fig.1 shows that, Meg starts to decompose significantly at 200 °C and undergoes a severe decomposition until 350 °C when the mass of Meg is just kept 12.2%. So the appropriate pyrolysis temperature for Meg to produce carbon dots should be lower than 300 °C. Otherwise a large amount of char that is difficult to disperse in water will be resulted due to the severe pyrolysis of Meg. For example, after pyrolyzed in a tube furnace at 300 °C for 2 h, the residual mass of Meg was about 34.6% and the resulting Py-Meg was difficult to completely disperse in water.

Benefitting from Gd(Ⅲ)-N-O cyclic chelate structure, the thermal stability of GdPA is higher than that of Meg, whose mass keeps upto 83.0% when heated to 350 °C (TGA, curve 2). The mass loss of about 17.0% is caused by the cleavage of two carboxyl groups that do not participate in coordination, and the Gd-N-O cyclic chelate structure mainly remains unchanged. It has been reported that when GdPA was heated at 250 °C for 2 h in air, the chelate structure within remained intact.[15] Furthermore, when GdPA was thermally treated in a tube furnace at 300 °C for 2 h, its residual mass was 86.5%, and the resulting Py-GdPA was well dispersed in water completely.

As a matter of fact the thermal behavior of GdPM exhibits some characteristics of Meg and GdPA because GdPM is a carboxylic acid ammonium salt composed of GdPA and Meg units (Fig.2). Seemingly, the TGA curve of GdPM (curve 3 in Fig.1) sits between that of Meg and GdPA. It is further intriguing that the mass loss of GdPM is much slower than that observed for a hypothetical TGA curve (curve 4). The hypothetical TGA curve is directly derived from a simple addition of the residual mass (RM) of Meg and GdPA (RM_{Meg}*196/744+RM_{GdPA}*548/744). It indicates that Meg with poor thermal stability becomes more stable after interaction with GdPA and forming GdPM. This can be further proved by a tube furnace test. When pyrolyzed in a tube furnace at 300 °C for 2 h, the residual mass of GdPM was about 78.3% which is higher than the linear additive residual mass of Meg and GdPA (72.8%, calculated method: 34.6%*196/744+86.5*548/744). We also found that after enduring the same pyrolysis process, the residual mass of equimolar Meg-GdPA mixture (i.e., mass ratio between Meg to GdPM is 196:548, named as Mx) is 75.7% which is higher than 72.8% too. Moreover, both the Py-GdPM and Py-Mx can be well dispersed in water completely to form a uniform and stable transparent suspension, distinctively differing from the Py-Meg and its mixture with Py-GdPA as well (Fig.S2). Therefore, it is inevitable that during the pyrolysis, the Meg and GdPA (unit) either in GdPM or in Mx will interact with each other. It is the interaction that ensures a single entity composed of Gd(Ⅲ) chelate and carbon dots.

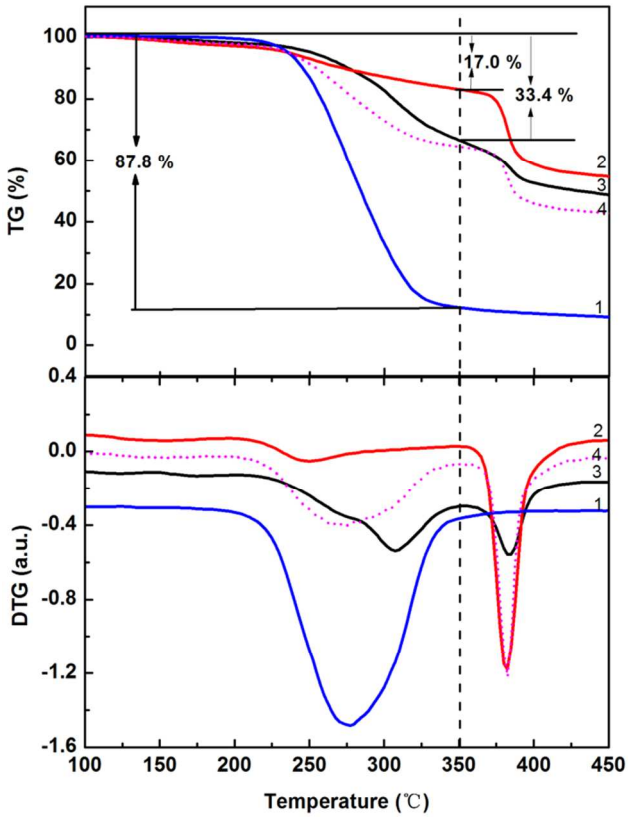

Fig.1 TGA and DTG curves (in N_2 atmosphere, heating rate: 10 °C/min. 1: Meg; 2: GdPA; 3: GdPM; 4: hypothetical curve).

Based on the above discussion, the temperatures for the pyrolysis of GdPM were roughly selected as 250 °C, 300 °C, 350 °C and 400 °C. Low temperature is unfavorable for decomposition and carbonization of GdPM, and excessively high temperature will promote the chelate structure to decompose. Compared the TGA and DTG curves of GdPM with those of Meg and GdPA, it can be concluded that during the heating process, the Meg unit with poor thermal stability decomposes prior to the GdPA unit; and the weight loss of GdPM below 350 °C (i.e. lower than 33.4%) is mainly caused by the decomposition of Meg unit.

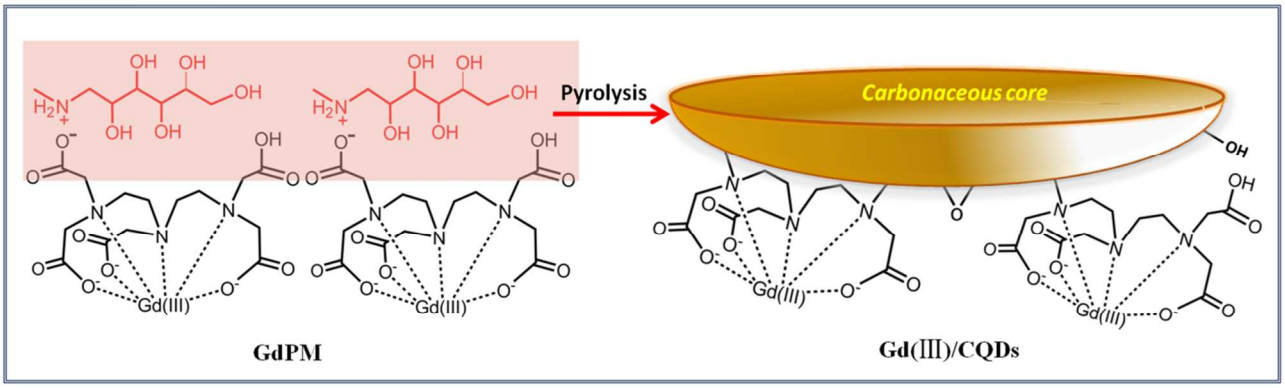

Fig.2 The molecular structure of GdPM and the sketched structure of resulting Gd(III)/CQDs.

3.2. Carbonization

The pyrolysis in a tube furnace led to volume expansion and mass loss of GdPM (white powder) and resulted in a brown product which can be partly dissolved in water indicating that GdPM was carbonized (Fig.3a). At the higher pyrolysis temperature, the color of carbonized product (Py-GdPM) was darkened and more non-dissolved residues were discarded. According to the TGA results, the mass loss lower than 33.4% is mainly attributed to the partial thermal decomposition of the Meg unit. When pyrolyzed in a tube furnace, the residual mass of GdPM decreases with the increase of pyrolysis temperature, a mass loss of 28.9% (residual mass71.1%) for GdPM pyrolyzed at 350 ^{o}C for 2 h is mainly ascribed to the partial thermal decomposition of its Meg unit, as shown in the residual mass-temperature curve of GdPM (Fig.4); a rapid decrease of residual mass appears when the temperature is above 350 ^{o}C indicating a different decomposition process, i.e., probably the Gd(Ⅲ) chelate structure starts to be pyrolyzed. So, we can say that when the GdPM is pyrolyzed at a temperature below 350 ^{o}C for 2 h, its Meg unit decomposes and is carbonized prior to cyclic Gd(Ⅲ) chelate structure.

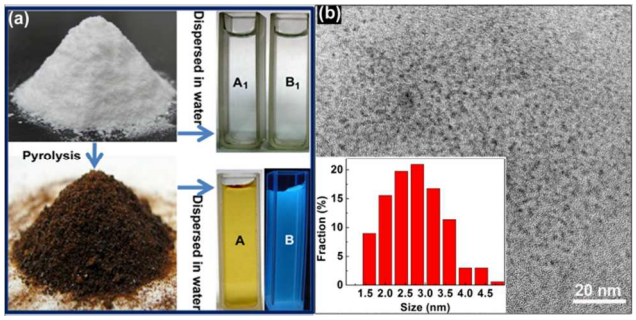

Fig.3 GdPM before and after be pyrolyzed (a), TEM image and size histogram for Gd(Ⅲ)/CQDs (b). A: without UV light; B: exposure to UV light.

3.3. Formation of Gd(Ⅲ)/CQDs

CQDs with stable dispersibility in deionized water were extracted from Py-GdPM, and it was found that the diameter of CQDs slightly increased with pyrolysis temperature. When the Py-GdPM was put into deionized water, a part of it was discarded as non-dispersible and the residual part could be well dispersed forming a yellow transparent dispersion. The yellow transparent dispersion exhibited blue fluorescence when irradiated with 365 nm UV light, while GdPM solution did not show any color when it was exposed to the same UV light (Fig.3a). TEM images show that diameters of the water-dispersed Py-GdPM prepared at 250 ^{o}C, 300 ^{o}C and 350 ^{o}C are 2.1 nm, 2.4 nm (Fig.S3) and 2.8 nm (Fig.3b), respectively. The nano-sized water-dispersed Py-GdPM those exhibit fluorescence are recognized as CQDs.[22]

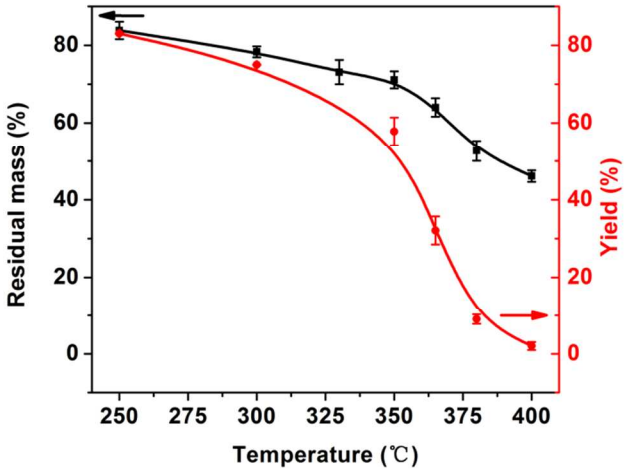

Fig.4 The residual mass of GdPM after pyrolysis by thermal treated constantly for 2 h (N_2 atmosphere, the heating rate in the stage from room temperature to pyrolysis temperature is 10 ^{o}C/min) and the yield of obtained CQDs.

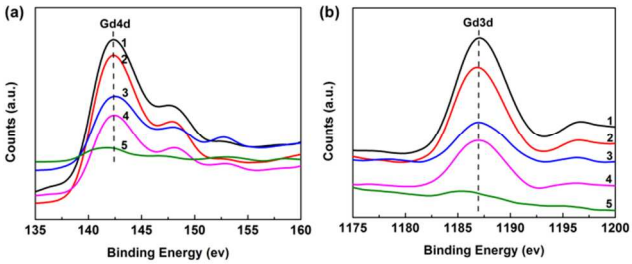

Fig.5 High resolution XPS spectra of Gd4d (a), and Gd3d (b), (1: GdPM; 2-5: CQDs prepared at 250 ^{o}C, 300 ^{o}C, 350 ^{o}C and 400 ^{o}C, respectively).

Although CQDs can be extracted from Py-GdPM prepared in a wide temperature range of 250-400 ^{o}C, it is better to keep the pyrolysis temperature not higher than 350 ^{o}C in order to obtain

Gd(III) chelates-doped CQDs. On the other hand, a lower pyrolysis temperature is beneficial for a higher yield of the CQDs. Free Gd(III) ions were detected in CQDs by dimethyl phenol orange, which were removed by forming precipitates with NaOH. Then the chelated Gd(III) ions were detected by XPS analysis. In the wide-scan XPS spectrum of CQDs prepared at 400 °C, no visible Gd4d or Gd3d peak appears, whereas the wide-scan XPS spectra of CQDs prepared at lower temperatures show main peaks attributed to C1s, O1s, N1s, Gd4d, along with Gd3d (Fig.S4). The high resolution XPS spectra of Gd4d and Gd3d in the CQDs prepared at temperatures of 250 °C, 300 °C and 350 °C show the same binding energy of 142.4 eV and 1187.0 eV as that of GdPM. It suggests that the coordination state and chemical environment of Gd(III) do not change significantly after pyrolysis[15]. However, the binding energies of Gd4d and Gd3d in CQDs prepared at 400 °C are decreased (Fig.5). The yield of the CQDs decreased gradually with the increase of pyrolysis temperature blow 350 °C depending mainly on the solubility of Py-GdPM; and a sharp decrease is observed above 350 °C down to 2.1% at 400 °C, as shown in Fig.4. At the pyrolysis temperature lower than 350 °C, only a few non-dissolved residuals in the Py-GdPM were discarded, especially for Py-GdPM obtained at 250 °C and 300 °C which were completely soluble in water; while lots of the Py-GdPM were discarded as non-dissolved when the pyrolysis temperature was higher than 350 °C. The small gap between residual mass of GdPM and the yield of CQDs at 300 °C as shown in Fig.4 is derived from the loss of Py-GdPM during centrifugation (to wipe off free Gd(III) ions) and concentration process.

Although a small amount of Gd(III) ions in GdPM are lost in the form of free ions during purification process after pyrolysis, the content of chelated Gd(III) in CQDs shows an inconspicuous decrease with the increase of pyrolysis temperature not higher than 350 °C. The mass concentration of chelated Gd(III) ions in CQDs was determined by ICP-ES and the results were listed in Table1. A small gap between the amount of chelated Gd(III) in CQDs prepared at 250 °C and that in GdPM was about 4.4%, and a smaller gap only about 0.8% existed between the amount of chelated Gd(III) in CQDs prepared at 350 °C and that prepared at 250 °C. However, when the pyrolysis temperature increased to 400 °C, the chelated Gd(III) content in CQDs was immediately reduced to 1.2%. These results suggest that only a small part of the Gd(III) chelate structure on the surface of the GdPM decomposed when the pyrolysis temperature was not higher than 350 °C; and a severe decomposition took place when the pyrolysis temperature was higher than 350 °C. Thermal-stable cyclic Gd(III) chelate structure could guarantee the chelated Gd(III) for CQDs at the lower pyrolysis temperature.

It is worth noting that, due to the interaction between the two structural units, the CQDs obtained at pyrolysis temperature of no higher than 350 °C were doped by chelated Gd(III) at a molecular level, which were named as Gd(III)/CQDs. In order to further demonstrate the point, we designed a dialysis experiment (detailed method was given in the Sec. 5 in the ESI). It is shown that the dialysis equilibrium attained quickly for the GdPA solution, whereas the Gd^{3+} concentration in dialysate retained a low level for the Gd(III)/CQDs solution. It is indicated that, in the Gd(III)/CQDs solution, most of the Gd^{3+} ions were chelated by CQDs that with diameters larger than the pore size of 1000D dialysis bag and thus difficult to pass through the dialysis bag; the small amount of Gd^{3+} ions presenting in the dialysate might be chelated by the smaller CQDs, as demonstrated by the UV-vis spectra of the dialysate. (Fig.S5).

Table 1 Chelated Gd(III) content, quantum yield (*QY*), and longitudinal relaxation rate (r_1) of CQDs prepared at different temperatures.

	CQDs				GdPM	Magnevist
	250 °C	300 °C	350 °C	400 °C		
Chelated Gd(III) content/wt.%	17.0	16.7	16.2	1.2	21.4	-
QY / %	2.6	3.4	8.9	12.5	0	0
*r_1 / mM·L^{-1}S^{-1}	6.4	6.1	5.5	-	6.5	4.7

*The r_1 was tested at the Gd(III) concentration of 0.5 mM.

3.4. Structure of Gd(III)/CQDs

Similar to the pyrolysis process of citric acid, glucose, L-lysine and other small aliphatic organic molecules, nano-sized carbonaceous cores are generated when the GdPM is used as a precursor for pyrolysis, though the carbonaceous cores are amorphous mainly. Bomlinos *et al.* proved that carbonized citric acid could produce graphite structures based on HRTEM and XRD analyses.[23] Mao *et al.* prepared carbon dots through hydrothermal method, and confirmed the graphite crystal structure of carbon dots by HRTEM.[24] Here, the carbonaceous cores in Gd(III)/CQDs are presented as amorphous carbon primarily due to the thermal-stable cyclic Gd(III) chelate structure which hinders the graphitization of GdPM during pyrolysis. As shown in Fig.6(a), the GdPM shows no diffraction peak, however two wide diffraction peaks at 2θ of 14.3° and 26.1° superimposed on a broad scattering background are observed in XRD curves of Gd(III)/CQDs, which can be attributed to intercalated graphite and graphite, respectively.[25] On the other hand, no diffraction peak belonging to new phase of free Gd(III) ions is found in the XRD patterns of Gd(III)/CQDs, indicating that the Gd(III) is stably coordinated with CQDs.

The Gd(III)/CQDs consist of a carbonaceous core containing both sp^2 and sp^3 hybridized carbon atoms and a Gd(III) chelates functionalized surface. As shown in UV-vis spectra of Gd(III)/CQDs, two absorption bands located at about 207 nm and 270 nm are attributed to π-π^* and n-π^* transition (Fig.6b), respectively, indicating the existence of sp^2 hybridized carbon atoms. These results are consistent with high resolution XPS spectra of C1s in Gd(III)/CQDs, where a C=C peak with a binding energy of 284.2 eV[26] is observed (Fig.6d). The Gd(III)/CQDs were prepared by incomplete carbonization of GdPM. The presence of sp^3 hybridized carbon atoms and carboxylate/hydroxyl moieties were revealed by C1s XPS high resolution spectra and IR spectra as shown in Fig.6c. The existence of carboxylate group further supports the presence of the Gd(III) chelates, which together with the hydroxyl groups endow Gd(III)/CQDs excellent dispersibility. In IR spectra, positions of main absorption peaks of Gd(III)/CQDs prepared at 250-350 °C show no obvious shift whereas the intensity of the absorption peak of –OH decreases. It implies that the chemical

structure of Gd(Ⅲ)/CQDs undergoes unobserved changes with pyrolysis temperature, accompanied by pyrolytic bond (i.e. –OH) cleavage.

Besides few influences on the content of chelated Gd(Ⅲ) ions, the pyrolysis temperature has a positive effect on the concentration of sp^2 hybridized carbon atoms in the carbonaceous core. In the UV-vis spectrum, the peak at 207 nm originating from the π-π^* transition of Gd(Ⅲ)/CQDs prepared at 250 °C is red-shifted with the increase of pyrolysis temperature and to 218 nm when the temperature is raised to 350 °C. In consistence with the UV-vis results, a temperature-dependent increase of C=C peak area shown in high resolution XPS spectra of C1s further suggests the increase of the concentration of sp^2 hybridized carbon atoms (Fig.6). However, due to the photoluminescence property, the Raman spectra of Gd(Ⅲ)/CQDs can hardly be obtained.

When GdPM was pyrolyzed at a temperature of 250-350 °C, the Meg unit performed as a growth centre for carbonaceous core, and the Gd(Ⅲ) chelate in GdPA unit functionalized on the surface of carbonaceous core. The structure of resulting Gd(Ⅲ)/CQDs was shown in Fig. 2.

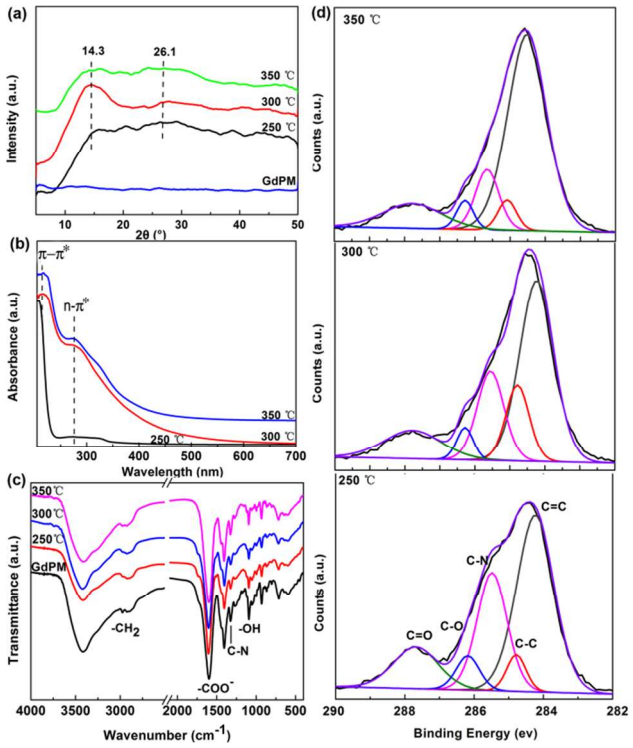

Fig.6 XRD patterns (a), UV-vis (b, λmax(250 °C, 300 °C, 350 °C)/nm: 207, 213, 218) and IR (c) spetra of Gd(Ⅲ)/CQDs prepared at different temperatures, as well as high resolution XPS spectra of C1s in Gd(Ⅲ)/CQDs (d).

3.5. Photoluminescence Properties of Gd(Ⅲ)/CQDs

Gd(Ⅲ)/CQDs can exhibit photoluminescence properties notably, a higher pyrolysis temperature can induce higher *QY* owing to the increases of the concentration of sp^2 hybridized carbon atoms. It is well known that either the increased concentration of sp^2 hybridized carbon atoms or the reduced particle size plays an important role in the increase of the *QY* of CQDs, though the extravagant concentration of sp^2 hybridized carbon atoms may lead to the luminescence quenching.[27, 28] In this view, the observed pyrolysis temperature-dependent increase in the *QY* (Table 1) may be attributed to the increased concentration of sp^2 hybridized carbon atoms. Since the particle size of CQDs increases with the pyrolysis temperature slightly as proved by TEM. Furthermore, these *QY* data suggest that the concentration of sp^2 hybridized carbon atoms does not reach its upper limit. Other methods (i.e. chemical reduction) should be developed to increase the concentration of sp^2 hybridized carbon atoms because excessive high temperature may accelerate the decomposition of cyclic Gd(Ⅲ) chelate structure and further restrain the formation of Gd(Ⅲ)/CQDs.

Gd(Ⅲ)/CQDs prepared at different temperatures exhibit PL spectra with approximately identical shape and peak position, and possess classic PL properties of excitation-dependent emission and pH-dependent emission intensity. The PL emission spectra (Fig.7a) recorded at an excitation wavelength of 350 nm (3.54 eV) show broad spectra centered at λmax ≈ 440 nm (2.82 eV) and with a Stokes shift of about 90 nm (0.72 eV). The large value of full width at half maximum (FWHM) of Gd(Ⅲ)/CQDs shows the presence of different types of fluorescent center with different emission λmax caused by the wide distribution of diameter. The Stokes shift here is smaller than that reported in literatures[21, 29] benefited from the surface carboxyl/hydroxyl moieties which play a role of passivator and facilitate more effective radiative recombinations.[27, 28] The PL excitation spectra show two excitonic bands centered at 368 nm (3.37 eV) and 396 nm (3.13 eV), as reported in Ref. [21]. The excitation-dependent PL emission behavior of Gd(Ⅲ)/CQDs is shown in Fig.7b. The normalized emission intensities show a red shift as the excitation wavelength increases. Also, we found that the Gd(Ⅲ)/CQDs have photoluminescent properties over a wide pH environment (pH =2-12) and the maximum emission intensity is obtained at a pH value of about 8 (close to the pH environment in the most of bodily fluids) which guarantees its clinical application possibility (Fig.7c,d). The maximum emission wavelength (λem), maximum excitation wavelength (λex), Stokes shift and FWHM of Gd(Ⅲ)/CQDs prepared at different temperatures are presented in Table S1.

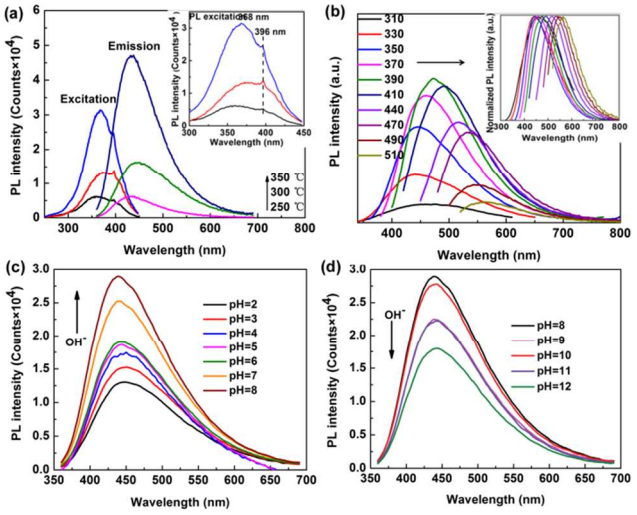

Fig.7 PL emission and excitation spectra of Gd(Ⅲ)/CQDs (a), excitation-dependent PL emission spectra (b), pH-dependent PL emission spectra (c: pH=2-8; d: pH=8-12).

3.6. Relaxation Properties of Gd(Ⅲ)/CQDs

Although the r_1 of Gd(Ⅲ)/CQDs slightly decreases with the increase of the pyrolysis temperature and is lower than that of GdPM due to

the loss of Gd(Ⅲ) on the surface during pyrolysis, it is obvious that the Gd(Ⅲ)/CQDs exhibit enhanced relaxivity and show higher r_1 compared to the clinical magnevist MRI contrast agent. As presented in Table 1, the r_1 of Gd(Ⅲ)/CQDs prepared at 250 °C is 6.4 $mM^{-1}\cdot S^{-1}$, which is almost the same as that of GdPM (6.5 $mM^{-1}\cdot S^{-1}$). When the pyrolysis temperature is up to 350 °C, the r_1 is reduced to 5.5 $mM^{-1}\cdot S^{-1}$ which is still higher than that of magnevist (4.7 $mM^{-1}\cdot S^{-1}$) containing the same content of Gd(Ⅲ). In addition, the symmetrically bright T_1-weighted MR images obtained by both coronal scan and axial scan (in Fig.8a) show that Gd(Ⅲ) ions were uniformly distributed in CQDs. The T_1 decreases linearly with the concentration of Gd(Ⅲ) in water, thus the signal intensity increases significantly, as shown in Fig.8b.

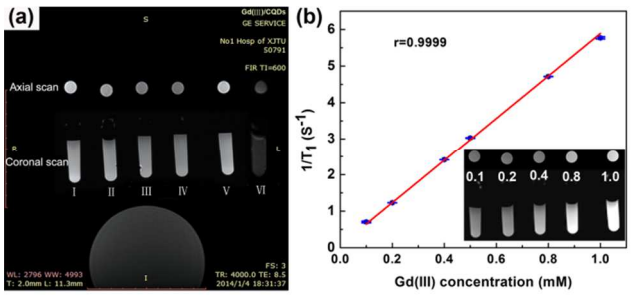

Fig.8 (a) T_1-weighted MR images of Gd(Ⅲ)/CQDs prepared at 250 °C, 300 °C and 350 °C (Ⅰ, Ⅱ, Ⅲ), magnevist (Ⅳ), GdPM(Ⅴ) ($M_{Gd(III)}$=0.5 mM) and water (Ⅵ). (b) Linear relationship between T_1 and Gd(Ⅲ) concentration for Gd(Ⅲ)/CQDs prepared at 300 °C in water. Inset: T_1-weighted images (T_1-weighted image of Gd(Ⅲ)/CQDs with Gd(Ⅲ) concentration of 0.5 mM has been shown in Fig.8a-Ⅱ).

3.7. Cytotoxicity and Cell Imaging

It is understandable that the Gd(Ⅲ)/CQDs do not show any serious cytotoxicity, because the Gd(Ⅲ) is stably chelated by biocompatible CQDs as proved above. Benefited from the surface carboxylate/hydroxyl groups, Gd(Ⅲ)/CQDs can be well dispersed in deionized water, phosphate-buffered saline buffer solution and culture medium without the assistance of ultrasonic vibration (Fig.S6). CCK-8 tests were conducted on human HeLa cells to evaluate the cytotoxicity of Gd(Ⅲ)/CQDs, as shown in Fig.9a. It is clear that Gd(Ⅲ)/CQDs show almost comparable cell viability at a concentration lower than 80 $\mu g\cdot mL^{-1}$. Furthermore, when HeLa cells were incubated in Gd(Ⅲ)/CQDs with the highest concentration of 200 $\mu g\cdot mL^{-1}$ for 24 h, the cell viability is still about 83%. As presented in Ref. [15], Gd(Ⅲ) doped carbon dots with concentration of lower than 200 $\mu g\cdot mL^{-1}$ shown low cytotoxicity for mouse fibroblasts cells. In comparison, some traditional semiconductor QDs showed toxicity even at a very low concentration.[30, 31]

Gd(Ⅲ)/CQDs possess the potential to be used as MRI/FI contrast agent due to its cell imaging applicability, as well as unconspicuous phototoxicity and cytotoxicity. The fluorescence images of cells incubated with Gd(Ⅲ)/CQDs at concentrations of 50 and 200 $\mu g\cdot mL^{-1}$ are shown in Fig.9c-d. The green fluorescence (excitation at 488 nm) in the cytoplasm region of HeLa cells is observed when the concentration of Gd(Ⅲ)/CQDs is 50 $\mu g\cdot mL^{-1}$, successfully demonstrating the uptake and applicability for cell imaging of Gd(Ⅲ)/CQDs. Furthermore, we find that higher dosage is beneficial for the uptake of Gd(Ⅲ)/CQDs and thus brightness of the green fluorescence, as shown in Fig.9d, a more bright green fluorescence is observed in both cytoplasm and nucleus of HeLa cells when the concentration of Gd(Ⅲ)/CQDs is increased to 200 $\mu g\cdot mL^{-1}$. However, it is better to control the dosage of Gd(Ⅲ)/CQDs in relative lower level (lower than 200 $\mu g\cdot mL^{-1}$) to avoid its affects on cellular activity. On the other hand, the Gd(Ⅲ)/CQDs will not induce any appreciable phototoxicity. Taking the viability of pristine HeLa cells as control (100%), the viability of HeLa cells that incubated without Gd(Ⅲ)/CQDs but exposure to blue light (470-480 nm, 1W) for 5 min and 10 min is 93.0% and 89.4%, respectively. It is exciting that the HeLa cells incubated with Gd(Ⅲ)/CQDs and exposure to blue light for 5 min and 10 min show comparable viability (91.0% and 90.1%, respectively) as shown in Fig.9b.

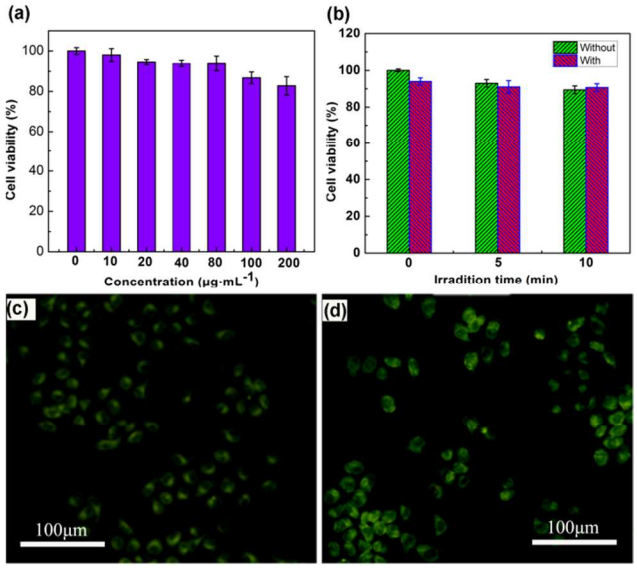

Fig.9. Viability of HeLa cells (a) incubated with various concentrations of Gd(Ⅲ)/CQDs for 24 h, (b) incubated with and without Gd(Ⅲ)/CQDs (50 $\mu g\cdot mL^{-1}$) and exposed to blue light (470-480 nm, 1W). Fluorescence microscope images (excitation at 488 nm) of HeLa cells after incubated with 50 $\mu g\cdot mL^{-1}$ (c) and 200 $\mu g\cdot mL^{-1}$ (d) Gd(Ⅲ)/CQDs for 20 h. The Gd(Ⅲ)/CQDs used here were that prepared under 300 °C.

4. Conclusions

We demonstrated a facile approach to prepare a magnetic resonance/fluorescence multimodal imaging contrast agent which is gadolinium(Ⅲ) chelates functionalized carbon quantum dots [Gd(Ⅲ)/CQDs]. The Gd(Ⅲ)/CQDs prepared by partial pyrolysis of gadopentetate monomeglumine (GdPM) at appropriate temperatures. The GdPM served as a precursor can provide both the carbon source and Gd(Ⅲ) source simultaneously. Gd(Ⅲ)/CQDs showed excellent wavelength-tunable fluorescence properties with the QY ~8.9% as well as superparamagnetic nature with the r_1 ~6.4 $mM^{-1}\cdot S^{-1}$ at room temperature. Cytotoxicity studies against HeLa cells showed noncytotoxic nature of Gd(Ⅲ)/CQDs, which together with the green fluorescence cell images indicating the possibility of utilizing the developed Gd(Ⅲ)/CQDs as a potential molecular imaging contrast agent.

Although high pyrolysis temperature is required to increase the carbonization degree and the amount of sp^2 hybridized carbon atoms to further increase the QY, it is preferable to keep the temperature not higher than 350 °C to avoid excess decomposition of cyclic Gd(Ⅲ) chelates. It will be a challenge to find another method to increase the sp^2 hybridized carbon atoms in Gd(Ⅲ)/CQDs without the loss of chelated Gd(Ⅲ).

Acknowledgements

This work is supported by the National Natural Science Foundation of China (No: 81171318) and Shaanxi Health Department Foundation, China (No: 2010E07).

Notes and references

[a] *Department of Applied Chemistry, School of Science, Xi'an Jiaotong University , Xi'an, 710049, China. Fax: +86 29 83237910; Tel.: +86 29 68640809; E-mail: xljing@mail.xjtu.edu.cn, rgfp-jing@mail.xjtu.edu.cn*

[b] *State Key Laboratory Cultivation Base for Nonmetal Composite and Functional Material, School of Materials Science and Engineering, Southwest University of Science and Technology, Mianyang, 621010, China.*

[c] *First Affiliated Hospital of Xi'an Jiaotong University, Xi'an, 710061, China.*

† Electronic Supplementary Information (ESI) available: some experimental details, supporting figures and tables. See DOI: 10.1039/b000000x/

1. R. Weissleder and M. J. Pittet, *Nature*, 2008, 452, 580-589.
2. D. K. Jones, D. Lythgoe, M. A. Horsfield, A. Simmons, S. C. Williams and H. S. Markus, *Stroke*, 1999, 30, 393-397.
3. X. Michalet, F. Pinaud, L. Bentolila, J. Tsay, S. Doose, J. Li, G. Sundaresan, A. Wu, S. Gambhir and S. Weiss, *Science*, 2005, 307, 538-544.
4. H. J. Weinmann, R. C. Brasch, W.-R. Press and G. E. Wesbey, *Am. J. Roentgenol.*, 1984, 142, 619-624.
5. P. L. Anelli, I. Bertini, M. Fragai, L. Lattuada, C. Luchinat and G. Parigi, *Eur. J. Inorg. Chem.*, 2000, 2000, 625-630.
6. M. Green, *Angew. Chem. Int. Ed.*, 2004, 43, 4129-4131.
7. J. Kim, Y. Piao and T. Hyeon, *Chem. Soc. Rev.*, 2008, 38, 372-390.
8. W. J. Mulder, R. Koole, R. J. Brandwijk, G. Storm, P. T. Chin, G. J. Strijkers, C. de Mello Donegá, K. Nicolay and A. W. Griffioen, *Nano Lett.*, 2006, 6, 1-6.
9. Y. Liu, K. Ai, Q. Yuan and L. Lu, *Biomaterials*, 2011, 32, 1185-1192.
10. H. Yang, S. Santra, G. A. Walter and P. H. Holloway, *Adv. Mater.*, 2006, 18, 2890-2894.
11. T. Jamieson, R. Bakhshi, D. Petrova, R. Pocock, M. Imani and A. M. Seifalian, *Biomaterials*, 2007, 28, 4717-4732.
12. S. T. Yang, L. Cao, P. G. Luo, F. Lu, X. Wang, H. Wang, M. J. Meziani, Y. Liu, G. Qi and Y. P. Sun, *J. Am. Chem. Soc.*, 2009, 131, 11308-11309.
13. B. Yin, J. Deng, X. Peng, Q. Long, J. Zhao, Q. Lu, Q. Chen, H. Li, H. Tang and Y. Zhang, *Analyst*, 2013, 138, 6551-6557.
14. S. Pandey, M. Thakur, A. Mewada, D. Anjarlekar, N. Mishra and M. Sharon, *J. Mat. Chem. B*, 2013, 1, 4972-4982.
15. A. B. Bourlinos, A. Bakandritsos, A. Kouloumpis, D. Gournis, M. Krysmann, E. P. Giannelis, K. Polakova, K. Safarova, K. Hola and R. Zboril, *J. Mater. Chem.*, 2012, 22, 23327-23330.
16. Y. Dong, J. Shao, C. Chen, H. Li, R. Wang, Y. Chi, X. Lin and G. Chen, *Carbon*, 2012, 50, 4738-4743.
17. A. Kundu, R. K. Layek, A. Kuila and A. K. Nandi, *ACS Appl. Mater. & Interfaces*, 2012, 4, 5576-5582.
18. S. Setua, D. Menon, A. Asok, S. Nair and M. Koyakutty, *Biomaterials*, 2010, 31, 714-729.
19. H. Yue, W. Wei, Z. Yue, B. Wang, N. Luo, Y. Gao, D. Ma, G. Ma and Z. Su, *Biomaterials*, 2012, 33, 4013-4021.
20. Y. Chang, S. T. Yang, J. H. Liu, E. Dong, Y. Wang, A. Cao, Y. Liu and H. Wang, *Toxicol. Lett.*, 2011, 200, 201-210.
21. S. Srivastava, R. Awasthi, D. Tripathi, M. K. Rai, V. Agarwal, V. Agrawal, N. S. Gajbhiye and R. K. Gupta, *Small*, 2012, 8, 1099-1109.
22. S. N. Baker and G. A. Baker, *Angew. Chem. Int. Ed.*, 2010, 49, 6726-6744.
23. A. B. Bourlinos, A. Stassinopoulos, D. Anglos, R. Zboril, V. Georgakilas and E. P. Giannelis, *Chem. Mater.*, 2008, 20, 4539-4541.
24. Y. Mao, Y. Bao, L. Yan, G. Li, F. Li, D. Han, X. Zhang and L. Niu, *Rsc Adv.*, 2013, 3, 5475-5482.
25. J. Shen, Y. Hu, M. Shi, X. Lu, C. Qin, C. Li and M. Ye, *Chem. Mater.*, 2009, 21, 3514-3520.
26. J. Diaz, G. Paolicelli, S. Ferrer and F. Comin, *Physical Review B*, 1996, 54, 8064.
27. L. Cao, M. J. Meziani, S. Sahu and Y. P. Sun, *Acc. Chem. Res.*, 2012, 46, 171-180.
28. G. Eda, Y. Y. Lin, C. Mattevi, H. Yamaguchi, H. A. Chen, I. Chen, C. W. Chen and M. Chhowalla, *Adv. Mater.*, 2010, 22, 505-509.
29. L. Tian, D. Ghosh, W. Chen, S. Pradhan, X. Chang and S. Chen, *Chem. Mater.*, 2009, 21, 2803-2809.
30. C. Wu, L. Shi, Q. Li, H. Jiang, M. Selke, L. Ba and X. Wang, *Chem. Res. Toxicol.*, 2009, 23, 82-88.
31. S. T. Stern, B. S. Zolnik, C. B. McLeland, J. Clogston, J. Zheng and S. E. McNeil, *Toxicol. Sci.*, 2008, 106, 140-152.

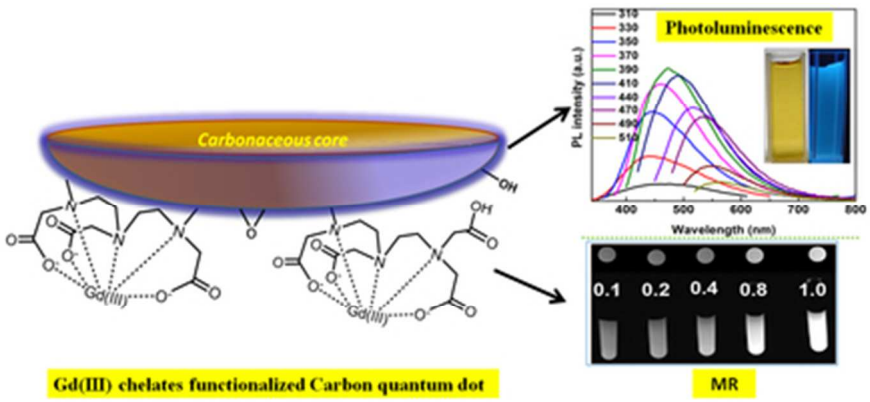

Gadolinium(III) chelates functionalized carbon quantum dots were prepared, which have good magnetic resonance response and photoluminescence properties can be used for multimodal imaging.
36x17mm (300 x 300 DPI)